Sādhanā (2023) 48:267
https://doi.org/10.1007/s12046-023-02340-8

Effect of solid/ball ratio and grinding time on the mechanical activation of kaolin

MERYEM GÖKTAŞ

Department of Metallurgy, Vocational College, Bilecik Seyh Edebali University, Bilecik 11230, Turkey
e-mail: meryem.goktas@bilecik.edu.tr

MS received 26 November 2022; revised 27 June 2023; accepted 20 October 2023

Abstract. Kaolin is one of the most important clay minerals that attracts attention due to its various application areas such as the ceramic industry. In this study, the effects of solid/ball ratio and grinding time on the mechanical activation of kaolin were investigated. Samples with 10 μm particle size were activated in The Fritsch Pulverisette 5 Ball Mill (Two Chamber Mill) at 400 rpm at different solid/ball ratios (1/10, 1/20, 1/30) and at different times (0, 15, 30, 45, 60 min.). The Planetary Ball Mill had 2 pieces of 80 ml tungsten carbide jar. Fritsch Pulverisette 5 was used in mechanical activation experiments and the planetary ball mill that can grind with the effect of impact/collision force. The X-ray diffraction (XRD) analysis results showed significant decrease in the intensity of the peaks after activation. The Fourier Transform Infrared Spectroscopy (FTIR) analysis spectra of the ground samples showed transformation to amorphous kaolinite. The results of the Scanning Electron Microscopy (SEM) with EDX analysis (SEM-EDS) analysis showed that in the unactivated kaolin, micro-size particles agglomerated among the larger particles. In the results of the particle size analysis and the Brunauer–Emmett–Teller (BET) analysis, it was observed that the specific surface area of kaolin increased as the grinding time increased. In the Thermogravimetric Analysis and Differential Scanning Calorimetry (TGA-DSC) analysis results, it was observed that the mass loss in mechanically activated samples occurred at lower temperatures. All the analysis results were examined and it was determined that the grinding time was more effective than the solid/ball ratio. It was concluded that the mechanical activation process of kaolin was more successful under the conditions 1/30 solid/ball ratio and 45 min. grinding time.

Keywords. Kaolin; ceramic; mechanical activation; solid/ball ratio; grinding time.

1. Introduction

Clay minerals are widely used in many areas of our lives such as geology, agriculture, construction, engineering, process industry and environmental applications. They are also used in plastics, drilling fluids, foundry bonds, chemical carriers, liquid barriers, decolorization, catalysis applications and the ceramics industry. Therefore, its traditional applications are quite numerous. In many of these applications, high purity, fine particle size and distribution, whiter and brighter colored clays with modified surface chemistry obtained by physical and chemical modifications are used. For this reason, the processing of raw kaolin in the ceramic industry is one of the important issues that have been emphasized in recent years [1, 2].

Mechanical activation is defined as the change in the reactivity of solids due to physicochemical changes during grinding and is one of the preferred methods for developing more environmentally processes to obtain new materials [3–8]. Mechanical activation of kaolin plays a key role in the preparation of ceramic raw materials. The partical size is reduced and thus the temperature is lowered during the sintering process.

The reason for this is that there is intense deterioration and partial amorphization in the structure due to excessive grinding. Grinding causes time-dependent physical property changes in terms of particle properties (morphology, (BET)), structure (crystal size), and surface charge (zeta potential) [9]. In addition, longer grinding time reduces the activation energy of the dehydroxylation process and thus the process takes place at lower temperatures [10, 11]. The variation of the grinding time affects the behavior of the structure.

Finally, the mechanical activation method is an environmental approach and provides superiority over chemical methods [9]. For this purpose, the effect of mechanical activation on kaolin ore below 10 μm particle size was investigated. The improvement of the structural properties of the mechanically activated kaolin ore with the effect of mechanical activation was emphasized. As a result, it is aimed at obtaining activated kaolin that can be used for various purposes in the ceramic industry. Thus, it is

Published online: 23 November 2023

predicted that the firing temperature will be reduced according to the findings obtained from the study.

2. Experimental

2.1 *Effect of solid/ball ratio and grinding time on mechanical activation*

Unactivated kaolin samples obtained under 10μm particle size was ground in the Planetary Ball Mill (Planetary Ball Mill) at 400 rpm. Dry grinding was carried out at different solid/ball ratios (1/10, 1/20, 1/30) and at different times (0, 15, 30, 45, 60 min.). By using the mechanical activation method [12, 13], amorphization was achieved in the structure of the kaolin mineral [14]. All samples were weighed using a Mettler Toledo brand AB104-S model precision balance. Photographs of planetary ball mill, jar and tungsten carbide balls were given in figure 1. The final size is <1 μm and has an operating speed of 50-400 rpm.

In this study, experiments were carried out both at different solid/ball ratios and at different grinding times. The effect of mechanical activation on the structural properties of the samples was investigated.

The flow chart of the experimental methods has been in figure 2.

In table 1, the experimental conditions (solid/ball ratio and grinding time) and codes of the mechanically unactivated and activated samples obtained during the experimental procedures were given.

2.2 *Characterization techniques*

XRF analysis was performed on raw samples to determine the major oxide components of the unground (raw) kaolin (SKO) sample. XRD, FTIR and SEM-EDS analyzes of the samples were performed before and after mechanical activation. The resulting mechanically non-activated and mechanically activated samples were characterized using X-Ray Diffraction (XRD, PAN analytical, 5–80° scanning range and 1°/min scanning speed with Empyrean instrument) and CuKα (λ=1.540590 Å) radiation. Fourier transform infrared spectroscopy analysis (FTIR) was performed

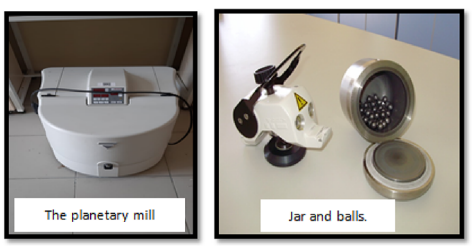

Figure 1. Photographs of the planetary mill, jar and balls.

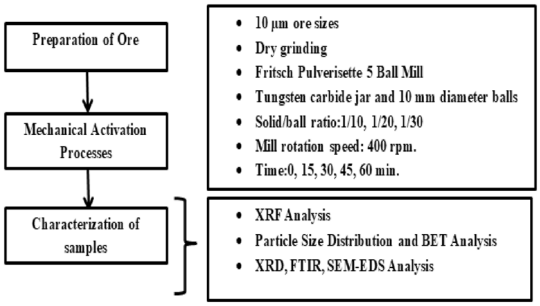

Figure 2. The flow chart of the experimental methods.

Table 1. Rates and codes of mechanically unactivated and activated samples.

Number of samples	Sample codes	Solid/ball ratio (weight %)	Grinding time (min.)
1	SKO	–	–
2	01-10-15	01/10	15
3	01-10-30	01/10	30
4	01-10-45	01/10	45
5	01-10-60	01/10	60
6	1-20-15	01/20	15
7	1-20-30	01/20	30
8	1-20-45	01/20	45
9	1-20-60	01/20	60
10	1-30-15	01/30	15
11	1-30-30	01/30	30
12	1-30-45	01/30	45
13	1-30-60	01/30	60

at room temperature using a Spectrum 100, Perkin Elmer spectrophotometer instrument in the wavenumber range of 400-4000 cm^{-1}. Scanning electron microscope (SEM) analysis to examine the surface properties was carried out using Zeiss Supra 40 VP brand SEM instrument at 5 kV voltage. Particle Size Distribution and Multipoint BET Surface Area analyzes were performed to characterize the samples obtained after mechanical activation. Thus, the obtained results were compared with the changes in the structures of raw kaolin and mechanically activated kaolin samples. In addition, thermal analyzes (TGA-DSC) of raw kaolin and mechanically activated kaolin samples were carried out in order to measure and interpret the changes in the properties of the samples as a result of physical and chemical reactions against temperature changes.

3. Results and discussion

3.1 *XRF and sieve fraction analyses*

In table 2 [15] and table 3, the XRF analysis results of the major oxide components of unground (unactivated) kaolin used in the study were given, respectively. The XRF

Table 2. Chemical analysis results of major oxide components of the SKO sample [15].

Chemical analysis	%
Na_2O	0.72
K_2O	2.39
MgO	0.35
CaO	0.44
Fe_2O_3	1.70
TiO_2	0.68
Al_2O_3	17.02
SiO_2	72.64
Loss of ignition	4.06
Total	100

Table 3. Physical analysis results of the SKO sample.

Particle size distribution	%
+10 mm	3
+6 mm	25
+3 mm	25
+1 mm	32
-1 mm	15
Humidity	% 5-8

analysis of the obtained unground kaolin (SKO) sample, it was observed that it has 72.64% SiO_2 and 17.02% Al_2O_3, 2.39% K_2O, 1.70% Fe_2O_3, 0.72% Na_2O, 0.68% TiO_2, 0.44 CaO and 0.35% MgO content by weight (table 2) [15]. The remaining weight-based % values were found to cause loss of ignition. Mebrek *et al* [2] stated that kaolin consists of two main chemical structures, SiO_2 (silica) and Al_2O_3 (alumina), and the loss of ignition was due to the presence of water in the mineral. The % Al_2O_3 content obtained from the XRF analysis results of the SKO sample given in table 2 demonstrates that it was a suitable clay raw material for ceramic applications. The physical analysis results given in table 3 were examined, it was observed that 32% of the SKO sample had +1 mm, 25% had +3 mm, and 25% had +6 mm particle size.

Particle size analysis of kaolin samples and the analysis of sieve fractions are important for ceramic production [16]. For this reason, sieve fraction analysis performed on SKO sample and the cumulative sieve curve was given in figure 3.

Figure 3 was examined, the sieve opening values corresponding to the d_{90}, d_{50} (average size) and d_{10} dimensions of the SKO sample, 100% of which were grounded below 10 mm, were determined, and the proportion of materials with a diameter of less than 6 mm was 97%, the proportion of materials with a diameter of less than 3 mm was 72%, the proportion of materials with a diameter of less than +1 mm is 47%, and the proportion of materials with a diameter of less than -1 mm was calculated as 15%. Considering the physical properties of the SKO sample, a clay mineral, it was observed that it was concentrated in smaller fractions below 6 mm [17].

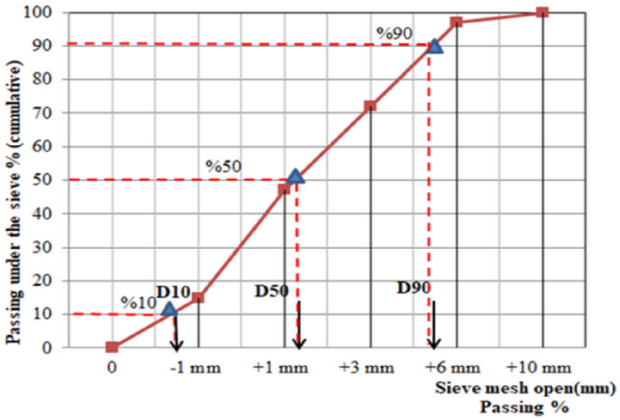

Figure 3. The cumulative sieve curve of the SKO example.

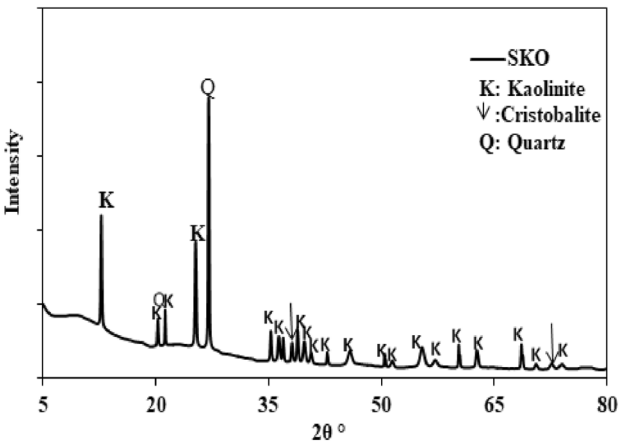

Figure 4. XRD analysis results of SKO sample [15].

3.2 *XRD analysis*

XRD analysis results of SKO (unground) and ground kaolin samples were given in figure 4 [15]. Figure 4 was examined, the peaks of kaolinite, indicated by K, were evidently observed from the SKO sample.

Figure 4 was examined, a large number of kaolinite peaks were detected in addition to the prominent peak of the SKO sample at 2θ°= ∼ 12.4° [15, 18]. In addition to the kaolinite (K) peaks, cristobalite ( ) and quartz (Q) peaks were evidently observed [15, 19].

In figures 5a–c, significant expansions and decreases in the intensities of kaolinite (K) peaks were recorded with

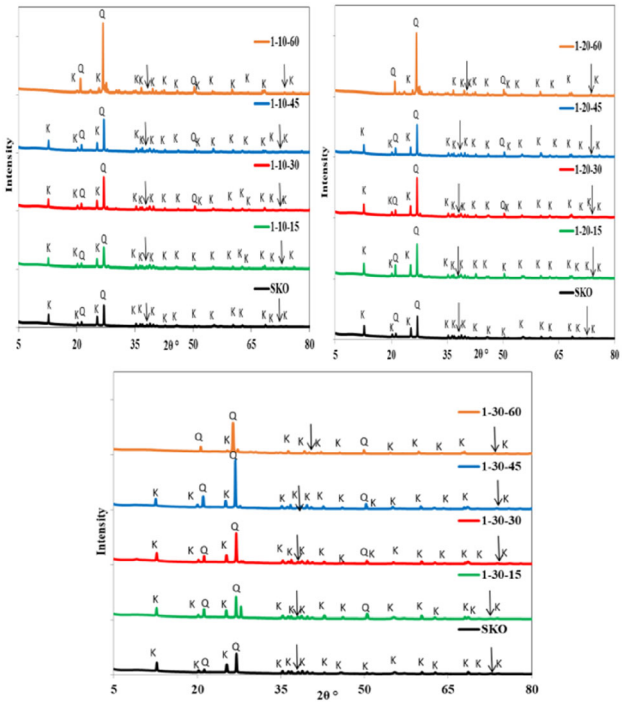

Figure 5. XRD analysis results of samples (a) SKO, 1-10-15, 1-10-30, 1-10-45, 1-10-60, (b) SKO, 1-20-15, 1-20-30, 1-20- 45, 1-10-60, (c) SKO, 1-30-15, 1-30-30, 1-30-45,1-10-60.

increasing grinding times with the mechanical activation process. The reason for this was the intense deterioration and partial amorphization of the structure due to mechanical activation. These reductions were consistent with the literature [15, 18, 20–23]. The increase in quartz (Q) peak with increasing grinding time showed that the mechanochemical activation of kaolin accelerated [15, 24].

The main purpose of mechanical activation was not only to remove water from the mineral [24], but also to weaken the lattice bonds by disrupting the crystal lattice structure [18]. Mechanical activation does not lead to complete dehydroxylation; however, it causes a significant deterioration and amorphization in the crystal structure of the clay mineral [1, 18, 22]. In short, the mechanical activation process was provided obtained with high efficiency of physical structure corrupted clay mineral [24].

Depending on the grinding speed (400 rpm/min.), the solid/ball ratio (1/10, 1/20, 1/30) and the grinding time (15, 30, 45 and 60 min.), the amorphization degrees of the kaolinite (K) mineral in the ground ore based on the XRD analysis were tried to be determined. Amorphization degrees of kaolinite (K) mineral were given in table 4.

The Amorphization Degree (%A) of mechanically activated kaolinite was calculated with the help of the formula given below, considering the kaolinite peaks as stated in the literature [22, 25, 26].

Table 4. Amorphization degrees of kaolinite (K) mineral in ground ore [15].

Mill speed, rpm/min.	Solid/ ball ratio	Grinding time, min.	Sample codes	% Degrees of amorphization
400	1/10	15	1-10-15	57.06
		30	1-10-30	60.22
		45	1-10-45	72.36
		60	1-10-60	77.71
	1/20	15	1-20-15	61.96
		30	1-20-30	65.19
		45	1-20-45	75.35
		60	1-20-60	79.24
	1/30	15	1-30-15	66.18
		30	1-30-30	79.07
		45	1-30-45	80.61
		60	1-30-60	84.49

$$\text{The Amorphization Degree} = 100 - [(\text{UoIx}/\ \text{IoUx}) \times 100]$$

Io is the area of the diffraction peak for the unground ore, Ix is the area of the diffraction peak for the ground ore, Uo is the ground value of the diffraction peak for the unground ore, and Ux is the ground value of the diffraction peak for the ground (mechanically activated) ore.

Table 4 was examined, it was observed that the percentage of amorphization increased as the grinding (mechanical activation) time and solid/ball ratio increased. The degree of amorphization after mechanical activation was calculated as 66.18%, 79.07%, 80.61% [15] and 84.49%, respectively (table 4) with respect to 1/30 solid/ball ratio at 15, 30, 45 and 60 min. The standard error of the amorphization degree of ground kaolinite samples was calculated as ±2%.

After 45 minutes of grinding, some of the kaolinite peaks disappeared. This has been attributed to the state of partial amorphization in existing crystal structures [27]. It was observed that the degree of amorphism increased with the mechanical activation process up to 60 minutes of grinding time (table 4) [15]. The obtained amorphous degree (A%) results and XRD patterns were evaluated together, and it was concluded that the sample with the code number 1-30-45 was the sample under the grinding conditions, especially where the kaolinite mineral was the most amorphous and the quartz mineral was the least amorphous. The kaolinite amorphous structure induced by grinding had reduced peak intensities. As a result, it was concluded that the grinding time of 45 minutes was sufficient for the mechanical activation process. The high SiO_2 (72.64%) content of the SKO sample (table 2) accelerated the mechanochemical process and increased the degree of amorphization [24, 25, 28].

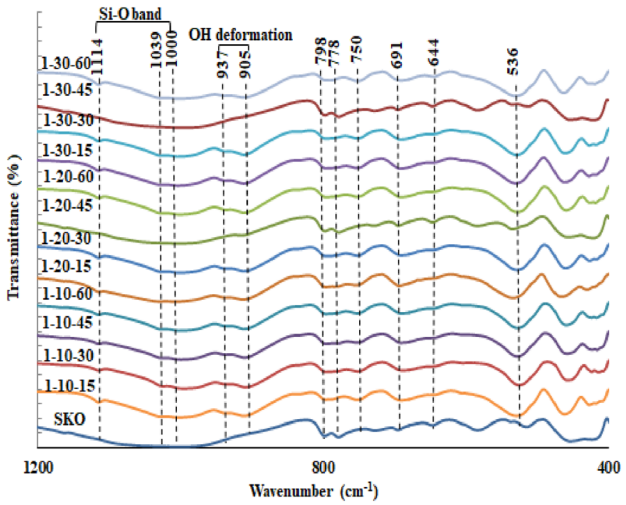

Figure 6. FTIR analysis results of activated samples and SKO (1200-400 cm^{-1}).

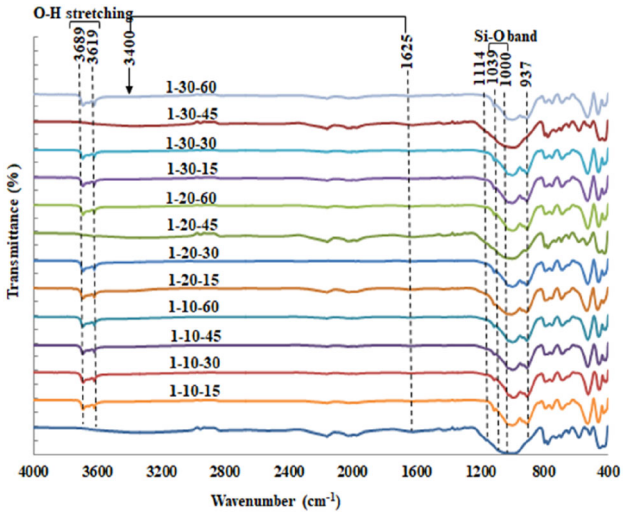

Figure 7. FTIR analysis results of activated samples and SKO (4000-400 cm^{-1}).

Because quartz particles acted as grinding bodies during the dry grinding of kaolinite [23].

3.3 *FTIR analysis*

FTIR analysis results of all samples were given in figure 6. The changes in the intensities of the defined bands were examined and the effect of the grinding time was explained. In the FTIR analysis, characteristic bending and stretching vibration bands were identified. Characteristic bands at (3600–3700) cm^{-1} representing the main absorption bands have been attributed to O–H stretching vibrations [20]. The peaks of three main characteristic bands at 3689, 3650 and 3619 cm^{-1} were identified. The number and location of these absorption bands were consistent with the literature [20, 21]. Although no band close to 3670 cm^{-1} was observed, the corresponding bands at 3689 and 3650 cm^{-1} were defined as basal hydroxyls. In the FTIR analysis in figure 7, characteristic bands at 3689, 3650, and 3619 cm^{-1} corresponding to SiO–H stretching vibrations were significantly reduced or disappeared in the band intensities of the mechanically activated samples; for 45 minutes no change was observed in the other bands. However, a significant increase in repetition band intensities was observed over 45 minutes. These increases were attributed to the reduction of in-phase surface hydroxyl vibrations [24].

Significant broadening of the bands at 3689 and 3619 cm^{-1} at 45 minutes grinding times was attributed to kaolinite amorphization [29]. These bands were attributed to the presence of residual kaolinite phases and that the OH groups remain bound between the kaolin layers [21]. The appearance of a broad band at 3443 cm^{-1} indicated hydroxyl vibration of adsorbed water, OH stretching and HOH deformation of the well-crystallized hydroxyl molecule with peaks in the range of 3400-1620 cm^{-1} [20, 21]. In addition, 3400 cm^{-1} and 1625 cm^{-1} O–H stretching bands were formed as a result of water bending vibration, not observed in figure 7 [20, 21]. It was stated that the grinding of kaolinite may cause a weak absorption band around 3400 cm^{-1}, but in this study, the presence of such a band was not found with increasing grinding times [20]. The weak band seen at 1114 cm^{-1} was attributed to apical oxygenated Si–O bonds in the OH plane [18, 20]. The region between 1000-1039 cm^{-1} was defined as SiO stretching region (Si–O bonds (Si with basal oxygen)).

The OH deformation of the region between 937-905 cm^{-1} was attributed to the Al–OH bending vibration hydroxyl modes of the bands at 910 and 938 cm^{-1}. These bands were also bands observed in both weak and very regular kaolinite structures [20]. The FTIR spectra of the ground samples were examined, no bands were found at 913 cm^{-1} indicating the presence of Al–O–H bonds. This showed that transformation to amorphous kaolinite and mechanochemical dehydroxylation had taken place [21].

Al–OH bending vibrations corresponding to these bands obtained at 60 minutes grinding times showed better resistance than O\H bands. The bands (Si–O bond) at 798, 778, 750 and 691 cm^{-1} were attributed to the presence of quartz [29], the band at 644 cm^{-1} was attributed to SiO deformations and octahedral sheet vibrations [20].

Regardless of the grinding time, the bands at 1039-905, 536 cm^{-1} were not observed over 45 min. [29]. With increasing grinding time, the decrease in peak intensities in the stress regions showed a scission of O\H bonds. In figure 6, it was seen that the decrease in peak intensities in the wavenumber range of 1200–500 cm^{-1} was weaker than in the OH stretching region [20]. Very weak bands in this range, after 60 min. of interval showed that after grinding, there were bonds between the OH groups and the kaolinite layers, that was, some residual kaolinite phase. However, as

the grinding time increased, these bands disappeared completely and the dehydroxylation process was completed. It was observed that the obtained FTIR analysis results supported the XRD analysis results (figure 4).

3.4 *SEM-EDS analysis*

Scanning Electron Microscopy (SEM) analysis was planned and the stage of determining the analysis conditions was initiated. In figure 8, the SEM image of the SKO-coded sample and the EDS analysis result were given. The SEM image of the SKO sample in figure 8 was examined at 1.000x magnification, it was seen that small-sized particals were located between large-size particles (large and small particles with irregular shapes in different sizes) [2, 15] and these particles had a leaf-like structure [15, 18].

In figure 9, SEM images of the mechanically activated samples at the same magnification (1.00KX magnification) were given. The SEM images (figure 9) of the samples with a low grinding time (15 and 30 min.) were examined, a decrease in particle size was observed with the effect of grinding, and it was observed that the smaller particles became more dominant with increasing grinding time (45 and 60 minutes) [15, 28]. The SEM images of all samples were evaluated together, it was seen that micron-sized particles were more prominent and the particles were randomly dispersed in kaolin samples subjected to the mechanical activation process for 45 minutes [1, 15, 28]. On the other hand, SEM images of samples subjected to mechanical activation for 60 minutes demonstrated agglomerated particles, proving the presence of more spherical-shaped, fused particles among randomly dispersed kaolin particles. Similar results had also found in the literature [22, 29].

In addition, the SEM-EDS analyzes of the 1-30-60 sample given in figure 10 were examined, a large amount of O as 50.11% by weight, Si as 29.53% by weight and Al as 17.96% by weight based on content distribution was observed.

Mako *et al* [24] and Tang *et al* [30] found that quartz (SiO_2) particles with a Mohs hardness of 7 (from the EDS analysis results given in figure 10) contributed to the mechanical activation of kaolin by acting as a grinding medium during dry grinding. The results of XRD, FTIR and SEM-EDS showed that the mechanical activation of the kaolin sample was successful.

XRD and SEM results showed that the structural properties of kaolin depend on the grinding time as well as the solid/ball ratio, and the grinding time was more effective than the solid/ball ratio on the mechanical activation of the kaolin. The analysis results were examined together, it was seen that the SEM results supported the XRD analysis results (figures 5a–c). In addition to the analyzes made, particle size analyzes were planned and the stage of determining the analysis conditions was started.

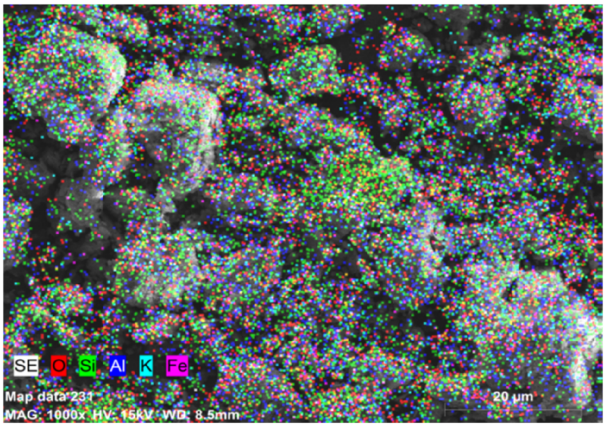

Figure 8. SEM-EDS analysis results of the SKO sample (1.000x)

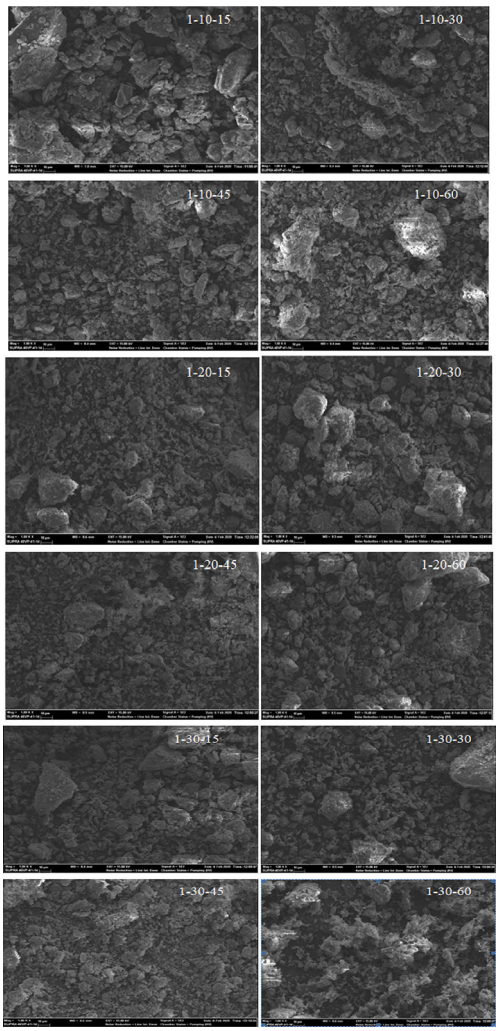

Figure 9. SEM analysis results of coded samples as 1-10-15, 1-10-30, 1-10-45, 1-10-60, 1-20-15, 1-20-30, 1-20-45,1-20-60, 1-30-15, 1-30-30, 1-30-45, 1-30-60 (1.00 KX).

Element	unn. C norm. C [wt.%]	norm. C [wt.%]	Atom. C [at.%]	Compound	norm. Comp. C [wt.%]	Error (3 Sigma) [wt.%]
Oxygen	18.45	50.11	63.78		0.00	8.67
Silicon	10.88	29.53	21.41	SiO2	63.18	1.52
Aluminium	6.61	17.96	13.55	Al2O3	33.93	1.07
Potassium	0.88	2.40	1.25	K2O	2.89	0.24
Iron	0.00	0.00	0.00	FeO	0.00	0.00
Total:	36.83	100.00	100.00			

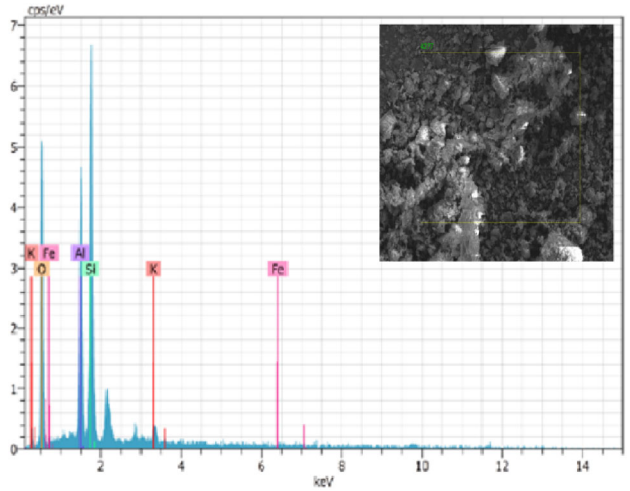

Figure 10. SEM-EDS analysis results of the 1-30-60 sample (1.000x).

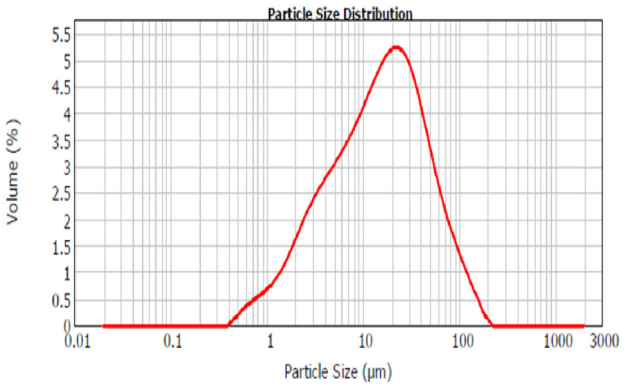

Figure 11. Particle size analysis of the SKO sample.

3.5 *Particle size analysis*

Particle Size Analyzes were performed using Malvern brand Mastersizer 2000 model particle size measuring instrument, which can measure particle sizes between 200 nm and 2000 µm. The graphs showing the particle size distribution obtained from the Particle Size Analysis results of the mechanically activated kaolin samples coded SKO and 1-30-60 were given in figures 11 and 12, respectively.

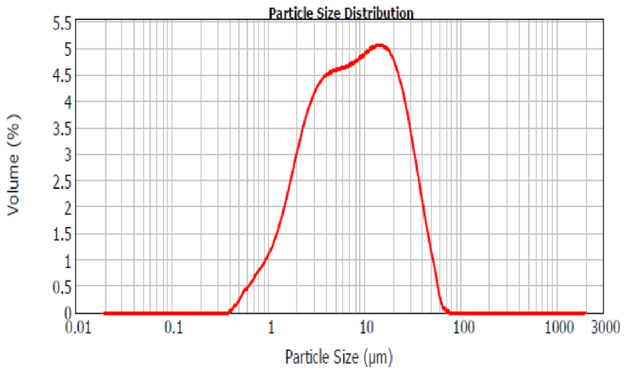

Figure 12. Particle size analysis of 1-30-60 coded mechanically activated kaolin.

Table 5. d10, d50 and d90 values of SKO and mechanically activated kaolin samples at different solid/ball ratios and different times.

Samples	d_{10}/µm	d_{50}/µm	d_{90}/µm
SKO	2.526	15.222	58.822
1-10-15	2.916	16.527	56.93
1-10-30	2.532	11.31	33.347
1-10-45	2.186	9.456	22.774
1-10-60	2.068	7.161	**28.675**
1-20-15	2.23	8.879	26.025
1-20-30	2.14	8.717	23.538
1-20-45	2.071	8.685	24.867
1-20-60	2.018	8.457	**28.256**
1-30-15	2.351	12.194	37.115
1-30-30	2.103	8.947	29.42
1-30-45	1.826	8.28	27.186
1-30-60	1.815	7.86	**28.357**

The data obtained from the particle size analysis results were examined, it was observed that the particle size of kaolin decreased with the mechanical activation process (increasing grinding times).

In addition, d_{10}, d_{50} and d_{90}values of SKO obtained from Particle Size Analysis and mechanically activated kaolin samples at different solid/ball ratios and different times were given in table 5. The d_{50} values given in table 5 and the SEM analysis results of the SKO sample were evaluated together, it was seen that it consisted of leafy particles with a value of 15.222 µm. After 60 minutes of grinding, the spherical particles increased and the leaf-shaped particles disappeared completely. Table 5 was examined, decreases in d_{50} values were observed with increasing grinding time. In figure 13, the effect of grinding times on d_{10}, d_{50} and d_{90} particle sizes of mechanically activated kaolin samples at different solid/ball ratios and different times were compared. Increasing grinding times caused to decreases in d_{10} and d_{50} values, it caused an increase in d_{90} values over 45 minutes of grinding time (Figure 13). The mechanic

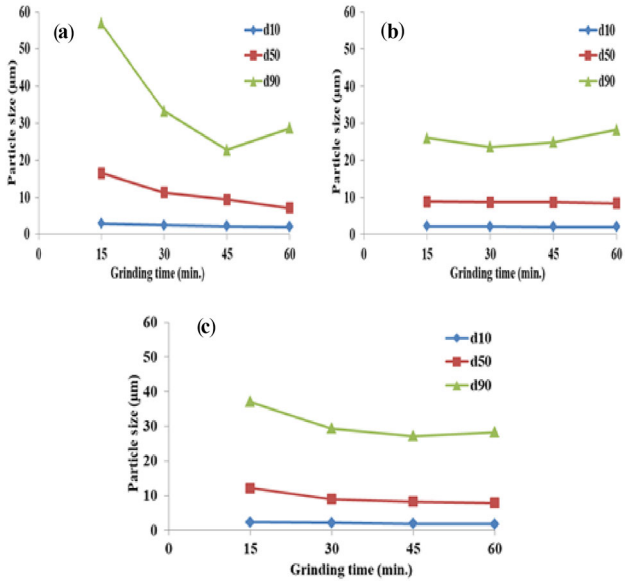

Figure 13. The effect of grinding time on d_{10}, d_{50} and d_{90} values of mechanically activated kaolin samples at different solid/ball ratios (**a**) 1/10, (**b**) 1/20 and (**c**) 1/30 and at different times (15, 30, 45, 60 min.).

activation process was importantly changed the morphology of the kaolin samples because of the repeated breaking and coalescenceof particles during grinding. d_{90} particle sizes of mechanically activated kaolin samples increased with grinding time up to 45 minutes and decreased slightly after 60 minutes of grinding as a result of particle agglomeration [29]. This indicated that the mechanical activation process had been carried out successfully. These results obtained were an indication that there was amorphization in the structure of kaolin with the mechanical activation process [29, 30]. The particle size analysis results were supported the XRD and SEM-EDS analysis results.

3.6 *BET surface area analysis*

Multi-point (7-point) BET (Brunauer–Emmet–Teller) Surface Analysis was used to determine the surface area in solids and the changes in the surface area of the mechanical activation process. BET Surface Analysis was carried out using the Micromeritics Gemini VII 2390 type instrument, with nitrogen (N_2) gas adsorption technique in a liquid nitrogen environment at -198°C. The results obtained were given in table 6. The BET Specific Surface Area distribution results of SKO and the mechanically activated kaolin samples at different solid/ball ratios and different times were examined in table 6, it was seen that the samples with smaller particle sizes have a larger surface area [31]. It was observed that the surface area of the kaolin increased during the 45 minutes grinding time. As seen in table 6, the surface area of the kaolin samples ground for 45 minutes increased more than the SKO sample. Figure 14 was

Table 6. BET analysis results of SKO and mechanically activated kaolin samples at different solid/ball ratios and different times.

Samples	Grinding time (min.)	S_{BET} Yüzey Alanı (m^2/gr)
SKO	0	10.1903
1-10-15	15	16.7013
1-10-30	30	18.2274
1-10-45	45	**23.1258**
1-10-60	60	15.479
1-20-15	15	11.9637
1-20-30	30	12.0246
1-20-45	45	**15.6357**
1-20-60	60	14.0583
1-30-15	15	10.6641
1-30-30	30	11.8524
1-30-45	45	**12.9001**
1-30-60	60	6.2164

examined, it was seen that the maximum value (23.1258 m^2/g) was reached after 45 minutes of grinding time (in the sample of 1-10-45), and it was determined that it decreased to 15.4790 m^2/g in a grinding time of 60 minutes (in the sample of 1-10-60) at a ratio of 1-10 by weight of solids/balls. It was observed that the surface area increased depending on the grinding time and the activated kaolin had a higher surface area compared to the unactivated kaolin [32]. The BET specific surface area at 1/30 solids/ball ratio for 45 minutes was found to be 10.1903 m^2/g for the SKO sample, and 12.9001 m^2/g for mechanically activated kaolin (table 6 and figure 14). The data obtained from the Partical Size Analysis results were examined together with the BET analysis given in table 6, the partical size of the kaolin decreased with the mechanical activation process (increasing grinding times) and accordingly the BET surface area increased. It was concluded that the decrease in the surface area value with the increased grinding time and solid/ball ratios (6.2164 m^2/g in mechanically activated kaolin for 60 minutes at 1/30 times/ball ratio) resulted from the agglomeration occurring between the particles [24, 29, 33]. Suraj *et al* [34] obtained results similar to those obtained in the BET Specific Surface Area analysis in figure 14.

N_2 adsorption isotherm curve and BET specific surface area graphs for SKO and 1-10-45 samples, respectively, were given in figures 15 and figure 16. The N_2 adsorption isotherm curves given in figure 16a and figure 16a were examined, it was seen that the amount of adsorbed N_2 gas gradually increases with increasing relative pressure (P/Po) [35]. In figure 15b, figure 16b and table 7, BET specific surface area values and pore volumes of SKO, 1-10-45 and 1-10-60 samples were compared. It was observed that the pore volume of the SKO sample given in table 7 was 2.4501 cm^3/g and the pore volume increased as the grinding

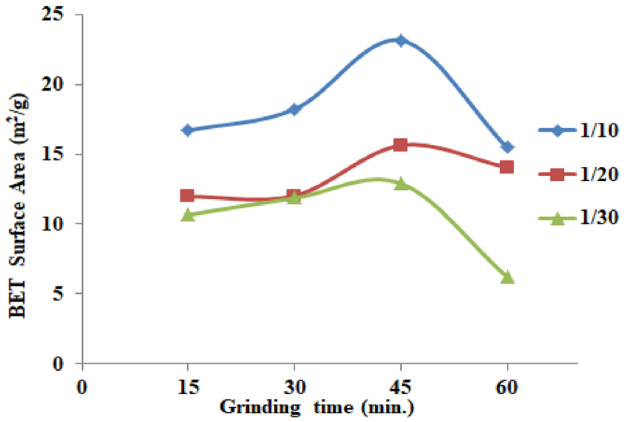

Figure 14. Effect of grinding time on BET surface area of mechanically activated kaolin samples at different solid/ball ratios (1/10, 1/20 and 1/30) and different times (15, 30, 45, 60 min.).

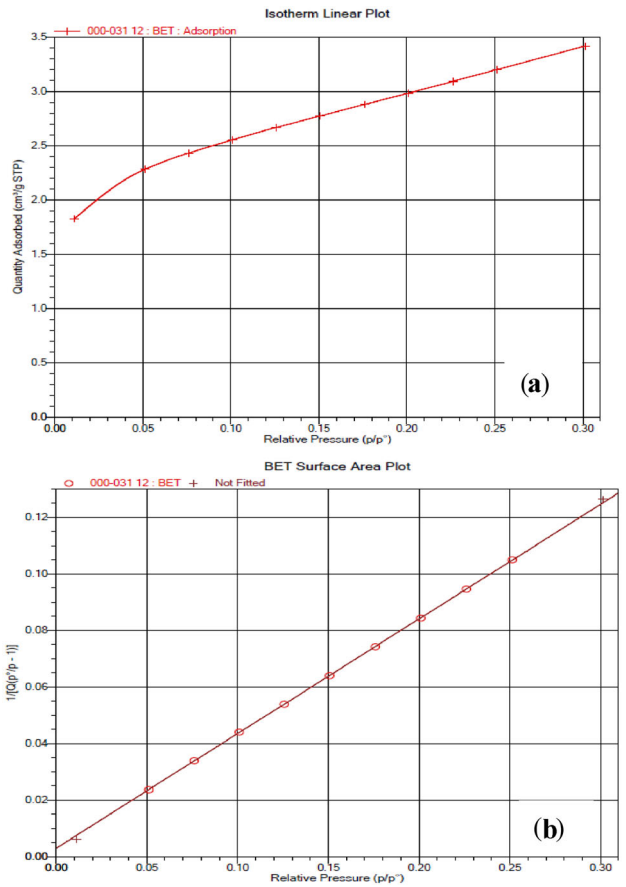

Figure 15. (**a**) N_2 adsorption isotherm curve and (**b**) BET specific surface area of the SKO sample.

time increased (5.3131 cm^3/g in the 1-10-45 sample) [36]. The BET Surface Area analysis results of the samples obtained were evaluated together, it was determined that the micro and mesopore volumes as well as the total pore

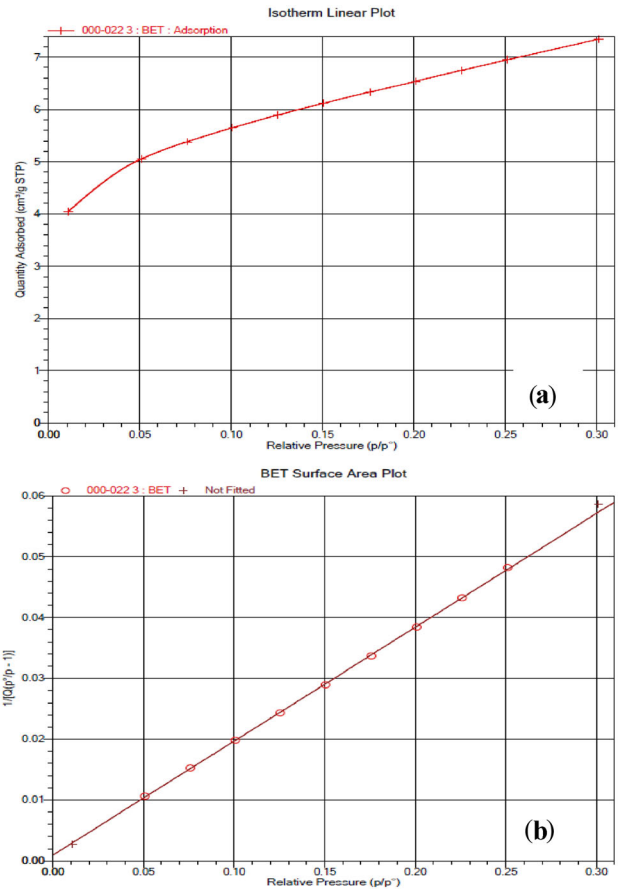

Figure 16. (**a**) N_2 adsorption isotherm curve and (**b**) BET specific surface area of sample 1-10-45.

Table 7. Comparison of BET specific surface area and pore volumes of SKO, 1-10-45,1-10-60 samples.

Sample codes	BET specific surface area/ (m^2/g)	Pore volumes/ (cm^3/g)
SKO	10.1903	2.4501
1-10-45	23.1258	5.3131
1-10-60	15.4790	3.5563

volume increased up to 45 minutes of grinding time. However, in samples ground for 60 minutes, this trend reversed (3.5563 cm^3/g) and decreased as a result of particle agglomeration (table 7) [29]. This was proof that while the particle size decreases with the mechanical activation process, the specific surface area and, accordingly, the pore volume increase [37]. It was concluded that changes in particle morphology and size during mechanical activation directly cause an increase in mesopore volume. On the other hand, it was determined that the mechanical activation process caused an increase in the micropore volume and

thus the total porosity, leading to the amorphization of the crystal structure of the kaolin mineral [37].

With the grinding process, the small pore on the surface of the particles was further enlarged and thus the specific surface area corresponding to the reactive surface was also increased. The effects of grinding time on the change of specific surface area and the degree of amorphization were examined together, it was observed that the degree of amorphization and the specific surface area values increased as the grinding time increased. However, the surface area value of kaolinite, which agglomerated in 60 minutes of grinding time, decreased as the grinding time increased [25]. In addition to the increase in the specific surface area of the over-ground minerals, their exposure to mechanical activation causes chemical or physicochemical transformations in their structures and affects the next process [12, 29]. The results of the XRD analysis showed that the samples were activated successfully, and the results of the SEM-EDS analysis showed that in the unactivated kaolin, the micro-size particles were agglomerated among the larger particles and had a particularly leafy structure. According to the results of Particle Size and BET Analysis; with the mechanical activation process, the particle size of the kaolin decreased and the surface area value increased accordingly. It was seen that the obtained BET Surface Area Analysis results supported the results of XRD, Particle Size and SEM Analysis.

3.7 *TGA-DSC (thermogravimetric) analysis*

TGA-DSC Analysis (Thermogravimetry analysis) results of mechanically activated kaolin samples at different solid/ball ratios and different times were given in figure 17. The TGA-DSC analysis results were examined, the following thermal events were observed: 1) At ∼100 °C, the mass loss occurred due to the loss of the body water of kaolinite and this situation lasted up to ∼350 °C due to the dehydration of the samples [1]. Mass loss due to dehydroxylation (transformation from crystalline phase to amorphous phase) was observed [38]. 2) Its structure was transformed into metakaolinite as a result of kaolinite dehydroxylation at ∼514 °C shown in the DSC curve characterized by an endothermic peak [39]. The changes in dehydroxylation temperature varied with grinding time and mass loss [10]. 3) The exothermic peak observed at ∼990 °C indicated the formation of a new crystalline phase called mullite (figure 17) [22, 40].

The exothermic peak observed in the SKO sample at ∼1005 °C was attributed to primary mullite formation. The same formation occurred at ∼990°C in the mechanically activated samples. This showed that the dehydroxylation of kaolinite increased with increasing grinding time [10]. Chen *et al* [39] stated in their study that the secondary mullite phase was formed at temperatures above 1300̊C and the crystallization of the secondary mullite phase increased

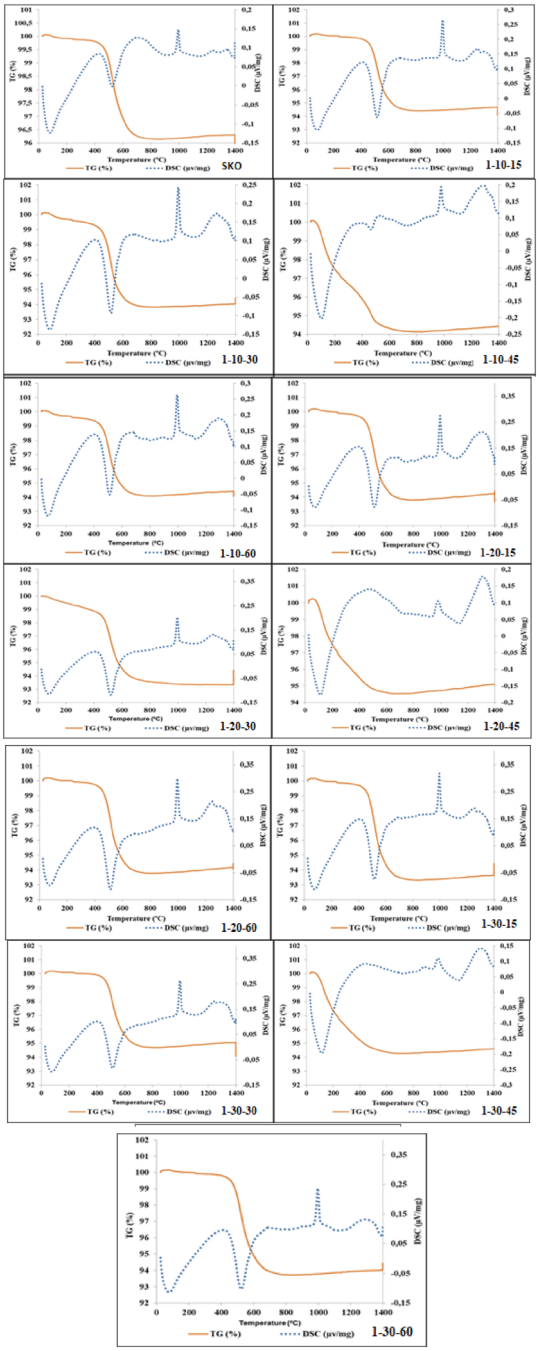

Figure 17. TGA analysis results of SKO and mechanically activated kaolin samples at different solid/ball ratios and different times.

with the addition of solid ratio (alumina). An exothermic peak indicating secondary mullite formation was observed at ∼1327°C in the SKO sample, the same peak was observed in the mechanically activated 1-30-45 sample at ∼1260 °C [22]. The peaks observed between 1150-1200°C were attributed to the crystallization of cristobalite from amorphous SiO_2 [41]. Over 1200 °C, a small exothermic peak was observed due to the formation of new phases, and

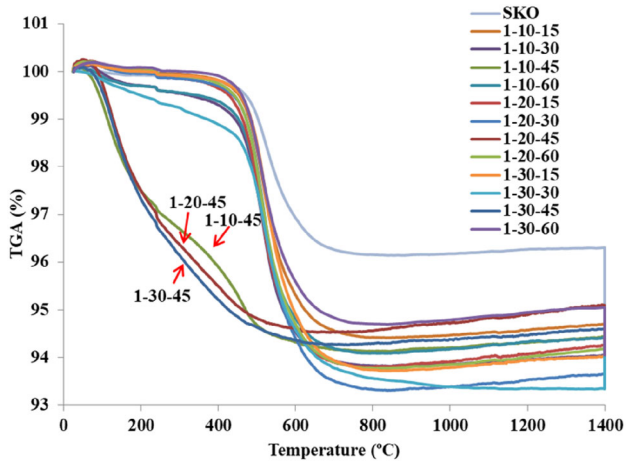

Figure 18. Comparison of TGA data of SKO and mechanically activated kaolin samples at different solid/ball ratios and different times.

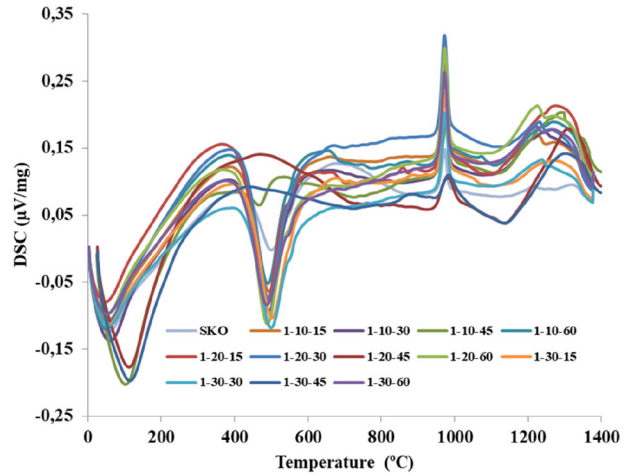

Figure 19. Comparison of DSC data of SKO and mechanically activated kaolin samples at different solid/ball ratios and different times.

this peak shifted to lower temperatures due to agglomeration due to the deformation of Si–O–Al bonds released during mechanical activation [25, 42].

In figure 18 and figure 19, SKO and TGA and DSC data of mechanically activated kaolin samples at different solid/ball ratios and different times were given comparatively. The SKO and TGA data of the mechanically activated kaolin samples at different solid/ball ratios and different times in figure 18 were examined, a mass loss of ∼0.8% was calculated due to the evaporation of the absorbed water and correspons to the first endothermic peak. Secondary mass loss was associated with a secondary endothermic peak at ∼514 °C, occurring between 450 °C and 750 °C (∼6%) and resulted from dehydroxylation of kaolinite [2, 14]. It was seen that the shift of the TGA curves in figure 18 to lower temperatures was proportional to the increasing grinding times. In figures 17, 18 and 19, where the results of TGA and DSC Analysis were given, were examined together, it was observed that the mass loss (maximum in the sample with code 1-30-45) occurred at lower temperatures due to the effect of excessive grinding in the mechanically activated samples. This showed that mechanical activation causes the formation of a new crystalline phase, mullite, at lower temperatures [20, 21, 43].

4. Conclusions

The effects of different solid/ball ratios and grinding times on mechanical activation were investigated by performing XRD, SEM-EDS, Particle Size Distribution, BET analyzes and TGA-DSC analyzes on SKO and mechanically activated samples. The results obtained from the study were given below.

- It can be seen from the XRD that the Intensity of peaks corresponds to Q increases with milling time, whereas peaks corresponds to K are almost same. This was due to the intense deterioration and partial amorphization of the structure due to mechanical activation.
- The FTIR spectra of the ground samples indicated transformation to amorphous kaolinite and mechanochemical dehydroxylation. Significant broadening of the bands at 3689 and 3619 cm^{-1} at grinding times of 45 minutes was attributed to kaolinite amorphization. The FTIR spectra of the ground samples were examined, no bands were found at 913 cm^{-1} indicating the presence of Al–O–H bonds. This indicated that transformation to amorphous kaolinite and mechanochemical dehydroxylation had taken place. It was observed that the peak intensities in the stress regions decreased with the increase of the grinding time. Weak bands in the 1200–500 cm^{-1} range indicated some residual kaolinite phase and bonds between the OH groups and the kaolinite layers after 60 minutes of grinding. However, as the grinding time increased, the disappearance of these bands showed that the dehydroxylation process was complete.
- SEM-EDS analysis showed that in unactivated kaolin, micron-sized particles were agglomerated among larger particles and consisted mainly of leaf-like structures. Micron-sized particles were found in the SEM images of the kaolin exposed to mechanical activation for 45 minutes, agglomerated particles were found among randomly dispersed kaolin particles in the SEM images of the kaolin samples subjected to mechanical activation for 60 minutes.
- Based on the particle size distribution analysis, the effects of grinding times on d_{10}, d_{50} and d_{90} particle sizes at different solid/ball ratios were compared. The d_{10}, d_{50} and d_{90} values of the samples obtained were

examined, it was observed that while increasing grinding time caused decrease in d_{10} and d_{50} values, it was seen that over 45 minutes of grinding time it caused an increase in d_{90} values due to agglomeration (60 minutes).

- The particle size analysis results and BET analysis results were examined together, it was observed that the specific surface area of kaolin increased as the grinding time increased. However, it was concluded that the decreases in the surface area values over 45 minutes grinding time (60 minutes) were due to the agglomeration that occurred between the particles (6.2164 m^2/g in mechanically activated kaolin for 60 minutes at a ratio of 1/30 times/ball ratio). According to the results of BET Surface Area and Particle Size Analysis, the surface area of the kaolin was increased by the mechanical activation process. Thus, kaolin, whose physical structure was amorphous by mechanical activation process, was obtained.
- According to the results of TGA-DSC Analysis performed to determine the mass change and thermal stability of all samples, it was observed that the mass loss occurred at lower temperatures in the mechanically activated samples with the effect of increasing grinding time.

All the analysis results obtained were examined together, it was concluded that the mechanical activation process of the sample obtained under grinding conditions with a solid/ball ratio of 1/30 and a grinding time of 45 minutes was more successful. As a result, it was concluded that the mechanical activation process was effective on the structural and surface properties of kaolin samples activated at different solid/ball ratios and grinding times.

Acknowledgements

The author thanks the financial support of the research foundation (Project no: 2021-01.BŞEÜ.11-05) of Bilecik Seyh Edebali University.

Declarations

Conflict of interest The author declares that there is no conflict of interest.

References

[1] Ondruška J, Csáki Š, Trnovcová V, Štubňa I, Lukáč F, Pokorný J, Vozár L and Dobroň P 2018 Influence of mechanical activation on DC conductivity of kaolin. *Appl. Clay Sci.* 154: 36–42

[2] Mebrek A, Rezzag H, Benayache S, Azzi A, Taïbi Y, Ladjama S, Touati N, Grid A S and Bouchoucha S 2019 Effect of chamotte on the structural and microstructural characteristics of mullite elaborated via reaction sintering of Algerian kaolin. *J. Mater. Res. Technol.* 8(5): 4010–4018

[3] Alex T C, Kumar R, Roy S K and Mehrotra S P 2014 Towards ambient pressure leaching of boehmite through mechanical activation. *Hydrometallurgy.* 144–145: 99–106

[4] Balaz P 2008 *Mechanochemistry in Nanoscience and Minerals Engineering*, Springer. Institute of Geotechnics Slovak Academy of Sciences Watsonova 45043 Kosice, Slovakia

[5] Balaz P, Achimovicova M, Balaz M, Billik P, Cherkezova-Zheleva Z, Criado J M, Delogu F, Dutkova E, Gaffet E, Gotor F J, Kumar R, Mitov I, Rojac T, Senna M, Streletskiikl A and Wieczorek-Ciurowam K 2013 Hallmarks of mechanochemistry: from nanoparticles to technology. *Chem. Soc. Rev.* 42: 7571

[6] Kumar S, Kumar R and Bandopadhyay A 2006 Innovative methodologies for the utilisation of wastes from metallurgical and allied industries. *Resour. Conserv. Recycl.* 48(4): 301–314

[7] Kumar R, Kumar S and Mehrotra S P 2007 Towards sustainable solutions for fly ash through mechanical activation. *Resour. Conserv. Recycl.* 52(2): 157–179

[8] Takacs L 2013 The historical development of mechanochemistry. *Chem. Soc. Rev.* 42(18): 7649–7659

[9] Singla R, Alex T C and Kumar R 2020 On mechanical activation of glauconite: Physicochemical changes, alterations in cation exchange capacity and mechanisms. *Powder Technol.* 360: 337–351

[10] Horváth E, Frost R L, Makó É, Kristóf J and Cseh T 2003 Thermal treatment of mechanochemically activated kaolinite. *Thermochim Acta.* 404(1–2): 227–234

[11] Ptácek P, Opravil T, Soukal F, Wasserbauer J, Másilko J and Barácek J 2013 The influence of structure order on the kinetics of dehydroxylation of kaolinite. *J. Eur. Ceram. Soc.* 33: 2793–2799

[12] Baláž P 2000 Extractive Metallurgy of Activated Minerals. 1st Edition. Elsevier

[13] Şener M and Erdemoğlu M 2014 Jipsin Isıl Davranışına Mekanik Aktivasyonun Etkisi. *Mining.* 53(3–4): 19–26

[14] Göktaş M 2018 Mechanical activation applications in mineral processing. *Mining.* 57(1): 57–66

[15] Göktaş M 2023 Effect of over grinding on the thermal behavior of kaoline of Bilecik/Söğüt region. *NOHU J. Eng. Sci.* 12(3): 990–997

[16] Ekmekçi Z, Gülsoy Ö, Ersayın S and Bayraktar İ 2001 Desulphurisation of İvrindi Alunitic Kaolin. *Bull. Earth Sci. Appl. Res. Centre Hacettepe Universit.* 23(22): 53–60

[17] Sánchez-Soto P J, Eliche-Quesada D, Martínez-Martínez S, Pérez-Villarejo L and Garzón E 2022 Study of a waste kaolin as raw material for mullite ceramics and mullite refractories by reaction sintering. *Mater.* 15(2): 583

[18] Leonel E C, Nassar E J, Ciuffi K J, dos Reis M J and Calefi P S 2014 Effect of high-energy ball milling in the structural and textural properties of kaolinite. *Cerâmica.* 60(354): 267–272

[19] Kart F 2007 Master of Science Thesis. Eskişehir Osmangazi University Department of Geological Engineering, Turkey

[20] Hamzaoui R, Muslim F, Guessasma S, Bennabi A and Guillin J 2015 Structural and thermal behavior of proclay kaolinite using high energy ball milling process. *Powder Technol.* 271: 228–237

[21] Mıtrovıć A and Zdujıć M 2013 *J. Serbian Chem. Soc*. 78(4): 579–590

[22] Yürüyen S 2011 *The Effect of Mechanical Activation on Cordierite Formation in Talc-Kaoline-Alumina Ceramic System*. Master of Science Thesis, Sakarya University, Turkey

[23] Göktaş M 2013 *Investigating the Effects of Intensive Milling on the Production of Synthetic Calcium Silicate from Marble Industry Wastes, by Using Ceramic Materials*. PhD Thesis, İnönü University, Turkey

[24] Mako E, Frost R L, Kristof J and Horvath E 2001 The effect of quartz content on the mechanochemical activation of kaolinite. *J. Colloid Interface Sci.* 244(2): 359–364

[25] Uysal T, Erdemoğlu M and Birinci M 2019 Effect of activation on aluminum recovery from pyrophyllite ore by acid leaching. *Mining.* 58(2): 111–120

[26] Akçay M and Apaydın M 2017 Investigation of the effect of mechanical activation on the leaching of malachite ore with ammonium nitrate. *AKU-J. Sci. Eng.* 17(2017): 717–726

[27] Makó É and Őze C 2022 The effects of silica fume and diatomaceous earth on the mechanochemical activation and pozzolanic activity of kaolin. *Appl. Clay Sci.* 228(106636): 0169–1317

[28] Aglietti E F, Porto Lopez J M and Pereıra E 1986 Mechanochemical effects in kaolinite grinding. II. Structural aspects. *Int. J. Miner. Process.* 16(1–2): 125–133

[29] Mıtrovıć A and Zdujıć M 2014 Preparation of pozzolanic addition by mechanical treatment of kaolin clay. *Int. J. Miner. Process.* 132: 59–66

[30] Tang A, Su L, Li C and Wei W 2010 Effect of mechanical activation on acid-leaching of kaolin residue. *Appl. Clay Sci.* 48(3): 296–299

[31] Ayalew A A 2020 Development of kaolin clay as a cost-effective technology for defluoridation of groundwater. *Hindawi Int. J. Chem. Eng.* 2020(8820727): 1–10

[32] Salahudeen N, Ahmed A S, Al-Muhtaseb A H, Dauda M, Waziri S M, Jibril B Y and Al-Sabahi J 2015 Synthesis, characterization and adsorption study of nano-sized activated alumina synthesized from kaolin using novel method. *Powder Technol.* 280: 266–272

[33] Sanchez-Soto P J, Haro M C J, Perez-Maqueda L A, Varona I and Perez-Rodrıguez J L 2000 Effects of dry grinding on the structural changes of kaolinite powders. *J. Am. Ceram. Soc.* 83(7): 1649–1657

[34] Suraj G, Iyer C S P, Rugmini S and Lalithambika M 1997 The effect of micronization on kaolinites and their sorption behaviour. *Appl. Clay Sci.* 12(1–2): 111–130

[35] Mustapha S, Tijani J O, Ndamitso M M, Abdulkareem S A, Shuaib D T, Mohammed A K and Sumaila A 2020 The role of kaolin and kaolin/ZnO nano adsorbents in adsorption studies for tannery wastewater treatment. *Sci. Rep.* 10(13068): 1–22

[36] Temuujın J, Burmaa G, Amgalan J, Okada K, Jadambaa T S and Mackenzie K J D 2001 Preparation of porous silica from mechanically activated kaolinite. *J. Porous Mater.* 8: 233–238

[37] Ilić B, Radonjanin V, Malešev M, Zdujić M and Mitrović A 2016 Effects of mechanical and thermal activation on pozzolanic activity of kaolin containing mica. *Appl. Clay Sci.* 123: 173–181

[38] Shvarzman A, Kovler K, Grader G S and Shter G E 2003 The effect of dehydroxylation/amorphization degree on pozzolanic activity of kaolinite. *Cem. Concr. Res.* 33(3): 405–416

[39] Chen Y F, Wang M C and Hon M H 2004 Phase transformation and growth of mullite in kaolin ceramics. *J. Eur. Ceram. Soc.* 24(8): 2389–2397

[40] Pinheiro D R, Gonçalves L R, Pacheco de Sena R L, Cruz Martelli M, Freitas Neves R, da Paixão Fernando and Ribeiro N 2020 Industrial kaolin waste as raw material in the synthesis of the SAPO-34 molecular sieve. *J. Mater. Res.* 23(2): 1980–5373

[41] Uysal T 2018 *Investigation of Activation Conditions in Alumina Production From Pyrophyllite Ore by Acid Leaching Method.* PhD Thesis, İnönü University, Turkey

[42] Fitos M, Badogiannis E G, Tsivilis S G and Perraki M 2015 Pozzolanic activity of thermally and mechanically treated kaolins of hydrothermal origin. *Appl. Clay Sci.* 116–117: 182–192

[43] Uysal T and Erdemoğlu M 2022 Production of aluminum titanate from pyrophyllite ore. *Journal of Polytechnic.* 25(1): 313–319